Journal of Material Cycles and Waste Management (2023) 25:826–834
https://doi.org/10.1007/s10163-022-01564-w

ORIGINAL ARTICLE

Flotation kinetics of aluminum powders derived from waste crystalline silicon solar cells and its comparison between batch, continuous and column flotation practices

Yoshiei Kato[1] · Sho Harada[1] · Noriko Nishimura[1] · Md. Azhar Uddin[1] · Yu-ichi Uchida[2]

Received: 22 June 2022 / Accepted: 27 November 2022 / Published online: 10 December 2022

Abstract

In this study, floatability rate of aluminum (Al) powders was analyzed for the purpose of separating valuable resources from residual materials in waste photovoltaic (PV) solar cells, and equations for flotation recovery were developed for various flotation types according to the rate-determining steps of the gas flowrate and feed rate. The flotation rate became a zero-order reaction at the rate-determining step of the gas flow rate and had the same form between a batch and continuous typed practices by substituting residence time with real time. Under the rate-determining step of the feed rate, the flotation rate was expressed by the linear combination of the first-order reaction of an even group material. The flotation recovery rate of Al powders was analyzed by the data of a batch floatability experiment and indicated by the linear expression of the first-order reaction of two groups due to the rate-determining step of the feed rate. The calculated separation recovery of *n*-cell type device increased as the number of cells increased and approached that of the batch and column types.

Keywords Flotation · Recovery · Waste solar cell · Column flotation · Cell-to-cell flotation

Introduction

Photovoltaic (PV) power generation is continuing to gain acceptance as one of the most effective means for controlling global warming. However, the most prevalent crystalline silicon solar cell modules are estimated to have a lifespan of 20–30 years, and end-of-life PV modules are expected to increase sharply in the near future. The EU (European Union) revised the WEEE (Waste Electrical and Electronic Equipment) directive [1, 2], under which re-use or recycling of waste PV modules was compulsory, and the Japanese government has also released a guideline on the recycling of waste PV equipment [3]. Although the frame and glass are relatively easily detached from the module for recycling, other parts such as ethylene vinyl acetate (EVA), silicon solar cells, electrodes, and wires are usually crushed together because they are difficult to separate. EVA has been successfully dissolved [4] or separated from other pulverized materials [5], and chemical etching processes using an acid or base solution have been applied as techniques for recycling valuable resources from residual pulverized silicon cell-containing materials [6–8]. The chemical composition of the inorganic element before the etching treatment was typically silicon (Si) of 87.5 mass%, aluminum (Al) of 9.5 mass%, silver (Ag) of 1.2 mass%, copper (Cu) of 0.5 mass%, tin (Sn) of 0.8 mass% and lead (Pb) of 0.3 mass% [9], which means that the separation between the Si and Al powders is important.

✉ Yoshiei Kato
y-kato@cc.okayama-u.ac.jp

Sho Harada
p0hh0n8d@s.okayama-u.ac.jp

Noriko Nishimura
nnoriko@okayama-u.ac.jp

Md. Azhar Uddin
alazhar@cc.okayama-u.ac.jp

Yu-ichi Uchida
yuichi.uchida@nit.ac.jp

[1] Department of Material and Energy Science, Graduate School of Environmental and Life Science, Okayama University, 1-1 Tsushima-naka, 3-chome, Kita-ku, Okayama 700-8530, Japan

[2] Department of Applied Chemistry, Faculty of Fundamental Engineering, Nippon Institute of Technology, 4-1 Gakuendai, Miyashiro-Machi, Minamisaitama-Gun, Saitama 345-8501, Japan

In recent years, flotation has also been applied to separation of waste mixed matter as a new field. Microwave [9–11], surface modification [12, 13], and Fenton pretreatments [14] were tried to an efficient flotation of plastic mixture. Hybrid jig which combined jig separation and flotation was developed to mixed-plastic wastes [15, 16]. Microplastics were recovered by a froth flotation technique [17, 18]. Flotation techniques were applicable to water clarification [19], ash treatment [20–22], and recycling of valuable metals such as gold [23–25]. With a view to separating valuable resources from pulverized silicon-based solar cells in large amounts, Harada et al. [26] proposed a flotation process and carried out batch laboratory-scale experiments with a mixture of Si and Al powders. Sodium dodecyl sulfate (SDS) which is an anionic surfactant permitted to hydrophobize Al powders alone due to the difference of surface potential between Si and Al, and behaved as a floating collector of Al. Flotation is a unit operation which is used in the mining industry to upgrade pulverized raw ore by introducing the ore into a solution containing a collector and supplying bubbles, and then recovering the hydrophobic valuable materials adhering to the bubble surface.

Many flotation kinetic models [27–29] have been proposed and evaluated to analyze flotation behavior, and reviews have also published [30–32]. One of the pioneering works on the flotation rate was done by Imaizumi and Inoue [33], who indicated that when sufficient bubbles exist in a pulp phase, the flotation rate of the focused powder group is represented by the sum of the rate of a small group of even powders, and flotation rate of each is proportional to its concentration, that is, it corresponded to the first order reaction. On the other hand, when the bubble surface is saturated with the focused powder group due to an insufficient supply of gas bubbles, the flotation rate corresponds to a zero-order reaction at the same gas flowrate, that is, the same bubble surface area. These explanations achieved an improvement of the *n*th-order flotation reaction with a different *n* value under different operation conditions. However, little research has been done on the difference of the flotation rates of various types of devices such as batch, one cell, *n*-cell (cell-to-cell), and column types.

In this study, aimed at an application of flotation technology to the recycle of waste pulverized Si solar cells, the effect of gas flowrate and Al feed rate on the rate-determining step of flotation recovery rate of depressed Al powders was discussed and the Al flotation rate was graphically illustrated by using the data of Harada et al. [26]. Next, depending on each rate-determining step, the temporal changes in the Al concentration of the pulp phase and recovery to the froth phase were calculated by the use of the same Al flotation rate constant for batch, continuous and column cells, and the results were compared.

Analysis of flotation kinetics

Rate-determining step of batch-typed Al flotation recovery

Harada et al. [26] investigated the effects of the air flowrate, collector concentration, ζ-potential of the powder surface, contact angle, pH, and mass ratio of Si to Al on flotation efficiency by batch tests of Si-Al powders. Recovery of the focused material (Al) decreased with a decreasing air flowrate and excessive collector concentration above the critical micelle concentration. The concentration or feed rate of the focused materials was also involved in the flotation rate [33]. In addition, Nguyen et al. [34] investigated the effect of turbulent environment such as sliding velocity and pulsation velocity of powders and bubbles on the flotation recovery.

As it is generally known, the flotation behavior of the focused *i* component caused by a bubble is shown schematically in Fig. 1. The hydrophobic and hydrophilic parts of the anionic (or cationic) collector adhere to the bubble and *i* component surface, respectively, and bubbles with the adhering *i* component rise to the froth. That is, separation of *i* and the other components is successfully achieved. A schematic diagram of metal flotation behavior in the pulp phase is shown in Fig. 2. Here, the feed rate of pulverized Metal A and gas flowrate were focused as operating variables and the other factors such as collector and frother concentrations, ζ-potential of the powder surface, and contact angle, were kept constant. Insufficient bubbles indicate that the bubble surface is covered with Metal A, which means that the rate-determining step of the flotation rate is the gas flowrate, whereas sufficient bubbles suggest that the collision velocity

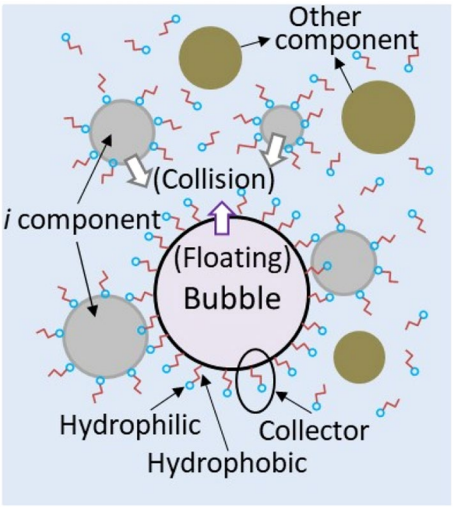

Fig. 1 Schematic diagram of metal flotation behavior caused by a bubble

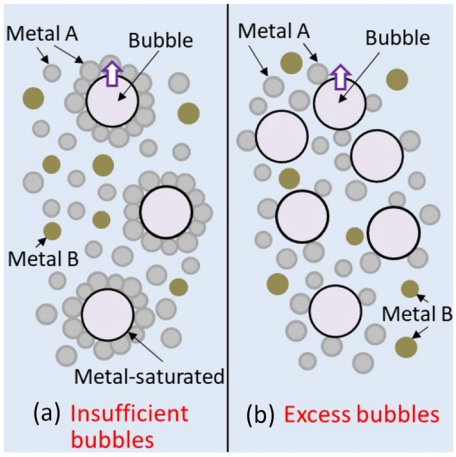

Fig. 2 Schematic diagram of metal flotation behaviors depending on rate-determining step

of the focused materials with bubbles is the rate-determining step of the flotation rate.

When the gas flowrate is the rate-determining step for the removal rate of the concentration, C_i [g L^{-1}], of the focused i component in the pulp layer, the $-\frac{dC_i}{dt}$ [g L^{-1} min^{-1}] value is supposed to be proportional to the two-thirds power of the gas flowrate, Q_{Air} [L min^{-1} (STP)], that is, the supplied rate of adsorbable surface area, as seen in Eq. (1).

$$-\frac{dC_i}{dt} = h_i Q_{Air}^{\frac{2}{3}}, \tag{1}$$

where h_i is the flotation rate constant of i component. The larger frother concentration and vessel volume reduces the bubble size and enhances the residual time of bubbles, respectively, which increases the flotation rate of i component at the same gas flowrate. The frother concentration and vessel volume affect the h_i term as operation variables, although they were kept constant in this study.

On the other hand, when the rate-determining step was the feed or feed rate of the i component, the $-\frac{dC_i}{dt}$ value became the sum of time-derivative of the concentration, $C_{i,j}$ [g L^{-1}], of an even j-group of powders in the focused i component, and $-\frac{dC_{i,j}}{dt}$ was proportional to $C_{i,j}$, as described by Imaizumi and Inoue [33].

$$-\frac{dC_i}{dt} = -\sum_{j=1}^{m}\frac{dC_{i,j}}{dt} = \sum_{j=1}^{m} k_{i,j}C_{i,j}, \tag{2}$$

where $k_{i,j}$ is the flotation rate constant when the rate-determining step is the feed or feed rate [min^{-1}] and m is the number of even group of powders.

The relationship between the rate-determining step, flotation controlling factor and removal rate of i-component concentration, C_i [g L^{-1}], in the pulp layer is summarized in Table 1. Integrating Eqs. (1) and (2) under $C_{i,0}$ [g L^{-1}] of the initial concentration of i component, Eqs. (3) and (4) were obtained, respectively, as follows.

$$\frac{C_i}{C_{i,0}} = 1 - \frac{h_i Q_{Air}^{2/3}}{C_{i,0}}t, \tag{3}$$

$$\frac{C_i}{C_{i,0}} = \sum_{j=1}^{m}\frac{C_{i,j,0}}{C_{i,0}}\exp\left(-k_{i,j}t\right), \tag{4}$$

where $C_{i,j,0}$ is the initial j group of the powder concentration in the focused i component [g L^{-1}].

From Eqs. (3) and (4), three possible temporal concentration changes are considered, as shown in Fig. 3a–c. The dash and solid lines denote the concentration changes with time for the rate-determining steps of a gas flowrate and a feed (rate), respectively. Figure 3a shows the case of the rate-determining step of a feed (rate) because the concentration of the solid line is always larger than that of the dashed one, whereas the dash line shows a permanent large concentration in Fig. 3b; that is, the rate-determining step is the gas flowrate. The rate-determining step in Fig. 3c changes from the gas flowrate in the early stage to the feed (rate) according to the concentration of the i component.

Flotation rates of batch, continuous stirred, and column typed devices

As shown in Fig. 4, the flotation efficiency of (a) batch, (b) 1-cell continuous stirred tank reactor (CSTR), (c) n-cell (cell-to-cell) CSTR, and (d) column types of flotation practices was analyzed under the same operation conditions. V is the vessel volume of the pulp layer [L], F_C is the supplied

Table 1 Relationship between rate-determining step, flotation controlling factor and flotation kinetics

	Rate-determining step	Flotation controlling factor	Flotation kinetics
I	Air flowrate	Bubble surface is saturated with particles	$-\frac{dC_i}{dt} = h_i {Q_{Air}}^{2/3}$
II	Feed or Feed rate	Collision between particles and air bubbles	$-\frac{dC_{i,j}}{dt} = \sum_{j=1}^{n} k_{i,j}C_{i,j}$

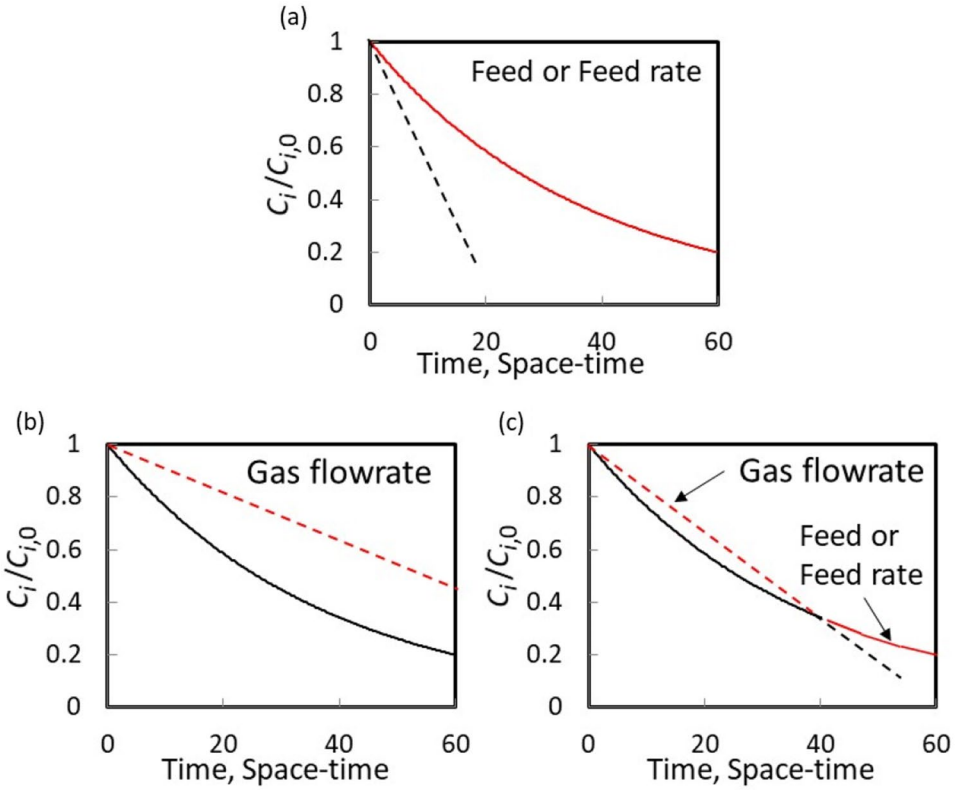

Fig. 3 Relationship between possible temporal changes in pulp layer concentration, and rate-determining steps of **a** feed (rate), **b** gas flowrate and **c** mixed controls

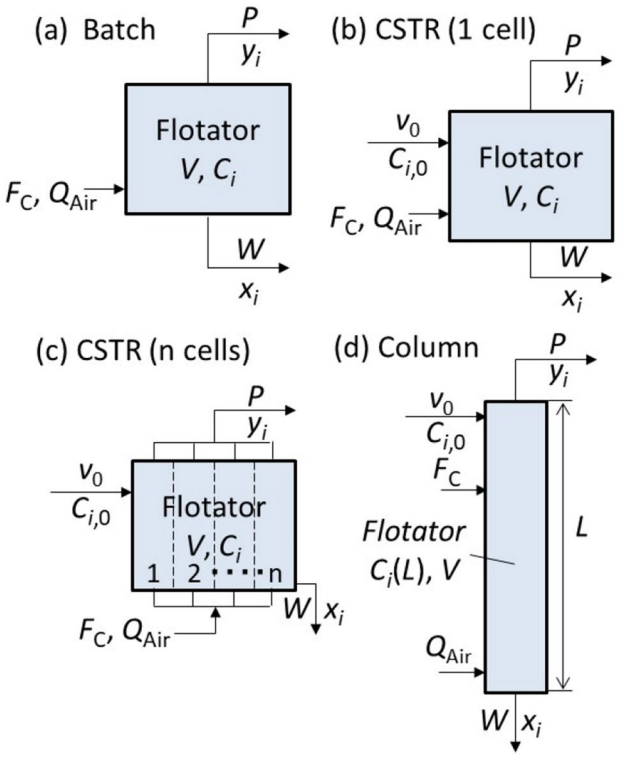

Fig. 4 Schematic diagram of 4 types of flotation practices and their state and operation variables

rate of the collector [g min^{-1}], P is the mass supplied rate of the i component to the froth layer [g min^{-1}], y_i is the mass fraction [-] of the i component in P, W is the mass supplied rate of waste (tailings) [g min^{-1}], x_i is the mass fraction of the i component in W, v_0 is the volumetric feed supplied rate [L min^{-1}]. The following section presents the equations for the recovery of the i component for flotation practices (a) to (d) in Fig. 4.

Flotation recovery of batch type

In the batch type flotator in Fig. 4a, the decreasing rate of the i component in the pulp layer is equal to the flotation rate because there is no feed input. Thus, Eqs. (1)–(4) are materialized, and the recovery, R_i [-], of the i component is given by Eq. (5) for the rate-determining step of a gas flowrate and by Eq. (6) when the feed in the pulp layer is the rate-determining step.

$$R_i = 1 - \frac{C_i}{C_{i,0}} = \frac{h_i Q_{\mathrm{Air}}^{\frac{2}{3}}}{C_{i,0}} t, \tag{5}$$

$$R_i = 1 - \frac{C_i}{C_{i,0}} = 1 - \sum_{j=1}^{m} \frac{C_{i,j,0}}{C_{i,0}} \exp\left(-k_{i,j} t\right). \tag{6}$$

Flotation recovery of 1-cell type

In the 1-cell type flotator shown in Fig. 4b, the mass balance for an even *j*-group of powders of the *i* component in the pulp layer is expressed by Eq. (7).

$$v_0 C_{i,j,0} - v_0 C_{i,j} + V\frac{dC_{i,j}}{dt} = 0. \tag{7}$$

The recovery value is introduced by substituting Eq. (1) for the rate-determining step of the gas flowrate and Eq. (2) for that of the feed rate into Eq. (7), as follows.

For the rate-determining step of a gas flowrate:

$$R_i = 1 - \frac{C_i}{C_{i,0}} = \frac{h_i Q_{\mathrm{Air}}^{\frac{2}{3}}}{C_{i,0}}\tau. \tag{8}$$

For the rate-determining step of a feed rate:

$$R_i = 1 - \frac{C_i}{C_{i,0}} = 1 - \sum_{j=1}^{m}\left(\frac{\frac{C_{i,j,0}}{C_{i,0}}}{1 + k_{i,j}\tau}\right). \tag{9}$$

Here, $\tau = \frac{V}{v_0}$ is the residence time [min] of the continuous flow system.

Flotation recovery of *n*-cells type

For the *n*-cells flotator in Fig. 4c, the *k* cell mass balance for an even *j*-group of powders of the *i* component in the pulp layer is represented by Eq. (10).

$$v_0 C_{i,j,k-1} - v_0 C_{i,j,k} + V_k\frac{dC_{i,j,k}}{dt} = 0, \tag{10}$$

where $C_{i,\,j,\,k\text{-}1}$ and $C_{i,\,j,\,k}$ are the *j*-group concentrations in the pulp layer of *k*-1 and *k* cells [g L^{-1}], respectively, V_k is the volume of the *k* cell [L].

R_i is summarized by Eqs. (11) and (12) for each rate-determining step.

For the rate determining step of a gas flowrate:

$$R_i = 1 - \frac{C_i}{C_{i,0}} = \sum_{j=1}^{m}\sum_{k=1}^{n}\left(\frac{C_{i,j,k-1} - C_{i,j,k}}{C_{i,0}}\right) = \frac{h_i Q_{\mathrm{Air}}^{\frac{2}{3}}}{C_{i,0}} n\tau_k = \frac{h_i Q_{\mathrm{Air}}^{\frac{2}{3}}}{C_{i,0}}\tau. \tag{11}$$

For the rate determining step of a feed rate:

$$R_i = 1 - \frac{C_i}{C_{i,0}} = 1 - \left(\frac{C_{i,1}}{C_{i,0}}\right)\left(\frac{C_{i,2}}{C_{i,1}}\right)\cdots\left(\frac{C_{i,n}}{C_{i,n-1}}\right) = 1 - \left(\sum_{j=1}^{m}\left(\frac{\frac{C_{i,j,0}}{C_{i,0}}}{1 + k_{i,j}\tau_k}\right)\right)^n. \tag{12}$$

Here, $\tau_k = \frac{V_k}{v_0}$ is the residence time [min] of *k* cell and $n\tau_k$ is equal to τ. τ_k is equal to τ

Flotation recovery of column type

The equation for a column flotator corresponds to that for a plug flow reactor. For a differential element of volume d*V* in the pulp layer in Fig. 4d, the mass balance for an even *j*-group of powders of the *i* component is given by Eq. (13) for the steady state.

$$v_0\frac{dC_{i,j}}{dV} = \frac{dC_{i,j}}{dt}. \tag{13}$$

R_i is obtained by integrating Eq. (13) with Eq. (1) for the rate-determining step of a gas flowrate and Eq. (2) for that of a feed rate as follows.

For the rate-determining step of a gas flowrate:

$$R_i = 1 - \frac{C_i}{C_{i,0}} = \frac{h_i Q_{\mathrm{Air}}^{\frac{2}{3}}}{C_{i,0}}\tau. \tag{14}$$

For the rate-determining step of a feed rate:

$$R_i = 1 - \frac{C_i}{C_{i,0}} = 1 - \sum_{j=1}^{m}\frac{C_{i,j,0}}{C_{i,0}}\exp\left(-k_{i,j}\tau\right). \tag{15}$$

Above Eqs. (14) and (15) are the same forms as Eqs. (5) and (6), respectively, for the batch flotator by substituting *t* of the batch process into τ of the column process.

Sections Flotation recovery of batch type to Flotation recovery of column type have shown that the R_i equation for the rate determining-step of a feed rate differed in each flotation system, whereas that for the rate-determining step of a gas flowrate was the same, as it is a zero-order flotation rate.

Results and discussion

Batch-typed Al flotation rate

The results of a batch test [26] with 2.5 g Al powder, 2.0 g L^{-1} sodium dodecyl sulfate (SDS) solution and 2.5 L min^{-1} (STP) air flowrate were analyzed to evaluate the rate-determining step of the depressed Al flotation and quantitatively express the floatability rate. The Al flotation recovery, R_{Al} [-], to the froth was defined by (weight of Al powders of the froth in the pan)/(weight of the initial Al powders in the pulp layer), which is equal to $(1 - C_{\mathrm{Al}}/C_{\mathrm{Al},0})$.

The temporal change of residue, $C_{\mathrm{Al}}/C_{\mathrm{Al},0} = 1 - R_{\mathrm{Al}}$, in the pulp layer is shown in Fig. 5 with the result of a mixture of Al/Si = 2.5 g/2.5 g [26]. The $C_{\mathrm{Al}}/C_{\mathrm{Al},0} = 0.18$ at 5 min in Fig. 5a was approximately the same as the $C_{\mathrm{Al}}/C_{\mathrm{Al},0} = 0.20$ for Al–Si mixture. Although entrainment generally plays an important role for multi-species, it was actually 3% for the Si–Al flotation experiment by Harada et al. [26]. It means

that the floatability results of the Al powders alone are applicable to those of the mixed powders such as Si and Al. Meanwhile, the lack of linearity in Fig. 5a indicated that the gas flowrate was not the rate-determining factor as denoted in Eq. (3). Moreover, from the lack of linearity in the semi-log plots in Fig. 5b, $C_{Al}/C_{Al,0}$ ($=1-R_{Al}$) was not represented by a simple first order reaction to the Al concentration, which means the floatability rate in this study must be analyzed by Eq. (4) considering the sum of an even group of powders.

Takamori and Fukami [35] proposed a simple method for the sequential calculation of flotation rate, $k_{i,j}$, of even j-group powders of an i component based on the assumption that an even group of powders with a lower flotation rate (lower $k_{i,j}$ value) continues to remain in the pulp layer. According to their method, the temporal change in Al flotation behavior was analyzed as shown in Fig. 6. The linear slope and t-intercept in Fig. 6 (a) were obtained from the line I of the multiple semi-log plots between longer experimental times, and then the line I values subtracted from the first plots were drawn as line II in Fig. 6b. When the straight line II included all the plots, as in this case, the operation was completed. This handling must be repeated for the curved line. In this study, the normalized concentration of the i component (Al) was given by the linear combination of the first-order reaction of two even group of powders as follows:

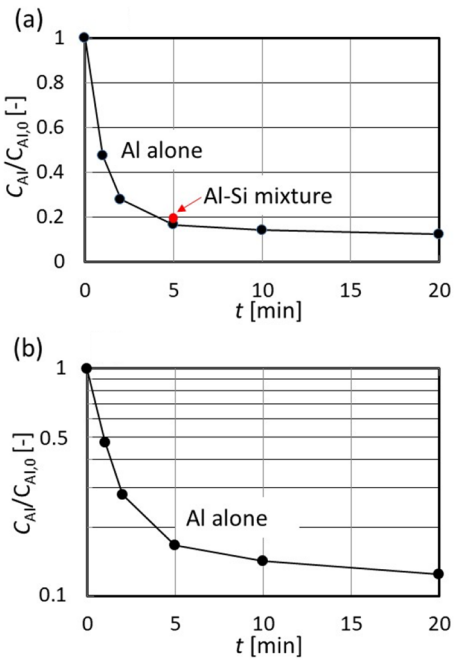

Fig. 5 Temporal changes in Al recovery and concentration in pulp layer

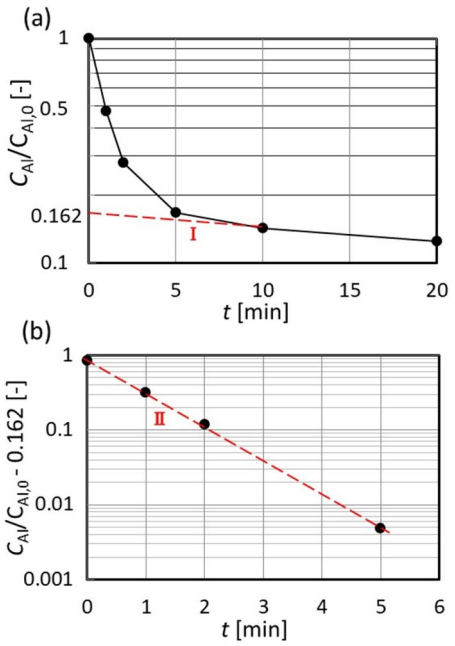

Fig. 6 Graphical method for rate constants of Al floatability

$$\frac{C_i}{C_{i,0}} = 0.838\exp(-0.986t) + 0.162\exp(-0.013t). \tag{16}$$

Assuming that the frequency of collision and adherence of Al powders to air bubbles is independent of the particle size, the flotation of the larger particle size proceeds more rapidly than that of the smaller one due to the heavier weight per particle. Thus, $C_{Al,1,0}/C_{Al,0}$ of 0.838 and $k_{Al,1}$, of 0.986 min^{-1} in the first term of the right-hand side in Eq. (16) indicate the larger size group, whereas $C_{Al,2,0}/C_{Al,0}$ of 0.162 and $k_{Al,2}$ of 0.013 min^{-1} in the second term the smaller size group. The Al powders were adjusted between 100 and 212 μm in this study. However, the Al sample with a wider size distribution might have a larger number of even group than $m=2$ in Eq. (16).

The above calculation procedure of $C_{i,j,0}/C_{i,0}$ and $k_{i,j}$ in this study will be also applicable to one of the tools for the analysis of flotation separation of mixed materials with different physical properties.

Comparison of batch, continuous mixed cell, and column type flotation practices

Temporal change in recovery for various flotation types

As a parameter of flotation rate constants, the temporal changes in recovery, R_i, for various flotation practices are shown in Fig. 7. $j=2$ and Eq. (17) were used for the rate-determining step of a feed (rate) as a guide for Eq. (16). That

is, the mass ratio of higher flotation rate of powders was set at 0.8 and that of lower one at 0.2.

$$\frac{C_i}{C_{i,0}} = 0.8\exp\left(-k_{i,1}t\right) + 0.2\exp(-k_{i,2}t). \quad (17)$$

The batch and column systems were unified into Fig. 7 (a) because the equation form was the same, as seen in Eqs. (5), (6), (14) and (15). Toward the constant $\frac{h_i Q_{\mathrm{Air}}^{2/3}}{C_{i,0}}$, the R_i for the rate-determining step of a gas flowrate resulted in the same line regardless of the type of flotators, as indicated in Eqs. (5), (8), (11) and (14). From Fig. 7, the R_i for the rate-determining step of a gas flowrate increased linearly with time, whereas that when the feed (rate) was rate-determining showed a decrease in the increase rate with time due to the lower powder concentration as shown in Eq. (1). Thus, even if the gas flowrate is controlling for R_i in the early stage due to the lower R_i, the feed (rate) becomes the rate-determining step after the time indicated by the intersection of the feed (rate) and gas flowrate.

In the cases of $(k_{i,1}, k_{i,2}) = (5, 0.05)$ and $(1, 0.01)$ of Fig. 7, R_i increased rapidly close to 0.8 and then became slow. It is because the powders group of the higher flotation rate with $k_{i,1}$ was almost removed to the froth layer until $R_i \approx 0.8$ and the lower flotation of the powders group with $k_{i,2}$ followed after that.

Comparison of recovery between flotation practices

The comparison of the temporal changes in R_i between the batch, n-cell CSTRs ($n = 1, 2, 3$), and column type flotation practices is shown in Fig. 8 for the rate-determining step of a feed (rate). The R_i curves of the batch and column types were always the highest, whereas that of the 1-cell device was the lowest. An increase in n in the n-cell CSTR resulted in a higher R_i, and R_i approached the values of the batch and column type flotators. The $\frac{V}{v_0}$ values required for the equal R_i increased the following ascending order: column, 3-cells, 2-cells, and 1-cell between the continuous flotation types, which means that the vessel volume of the column type is the smallest at the same feed rate.

Therefore, it is concluded that the most preferred flotation separation of Al powders is the column type practice under the rate-determining step of feed rate.

Conclusions

Flotation recovery rates of depressed metallic powders were examined for batch, continuous and column types of flotation practices under the rate-determining steps of a gas flowrate and a feed (rate).

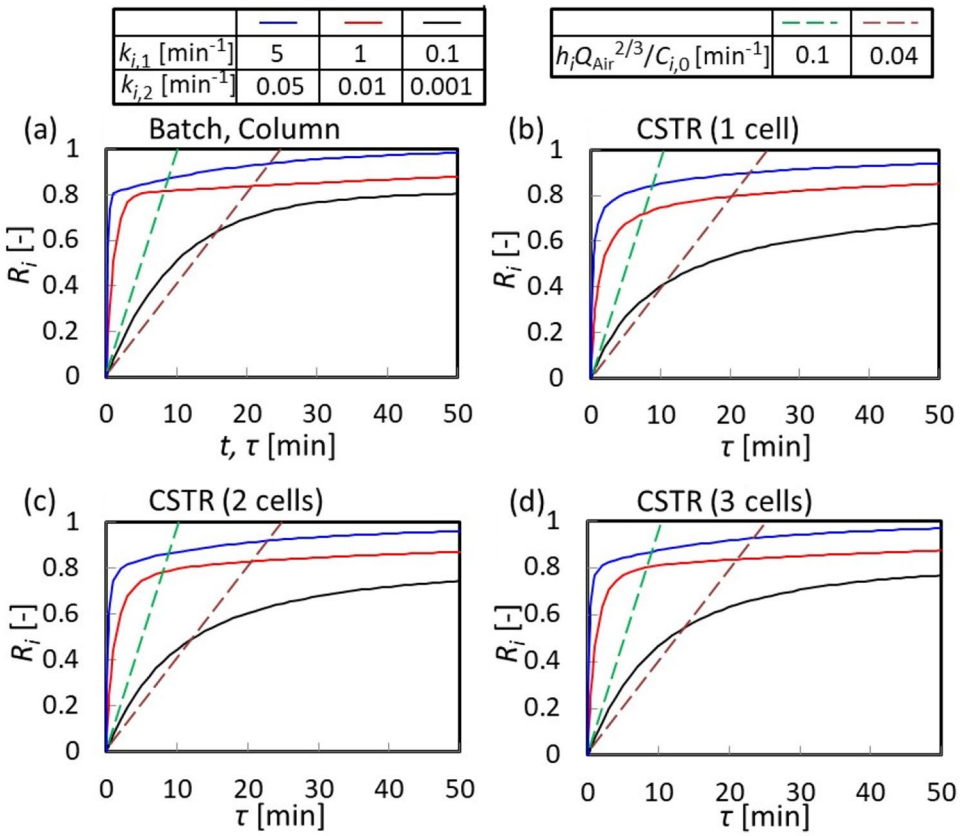

Fig. 7 Calculated temporal changes in recovery for various types of flotation practices

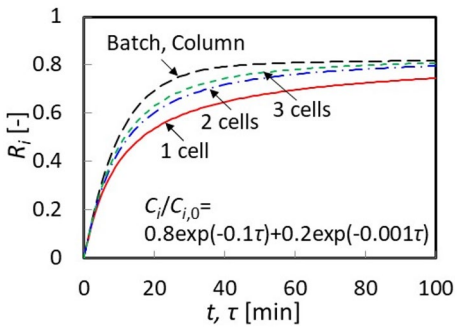

Fig. 8 Comparison of calculated recovery for equal flotation factors between various types of flotation practices under rate-determining step of feed (rate)

(1) The flotation recovery rate increased linearly with increasing real- or residence-time under the rate-determining step of a gas flowrate, whereas it was represented by the sum of the concentrations of even *j*-group of floating materials for the rate-determining step of a feed (rate).
(2) The rate-determining step for the flotation recovery rate changed to the feed (rate) at the later time stage, even if it was the gas flowrate at the early time stage. It is due to the smaller concentration of the froth component and lower flotation rate.
(3) The floatability rate of Al powders was successfully analyzed based on a batch experiment and expressed by the linear combination of the first-order reaction of two groups under the rate-determining step of a feed.
(4) The equations of the flotation recovery rate were proposed and calculated for the batch, 1-cell, *n*-cell and column types under the rate-determining steps of the gas flowrate and feed (rate).
(5) In the flotation calculations, the flotation rate of the batch type had the same form as that of the column type under the rate-determining step of a feed (rate). The flotation recovery of the *n*-cell CSTR type increased with the increasing cell number and approached that of the batch and column types.

Declarations

Conflict of interest The authors declare that they have no conflict of interest.

References

1. Union E (2012) Directive 2012/19/EU of the European parliament and of the Council of 4 July 2012 on waste electrical and electronic equipment (WEEE). Off J Eur Union 197:38–71
2. Dias P, Schmidt L, Gomes LB, Bettanin A, Veit H, Bernardes AM (2018) Recycling waste crystalline silicon photovoltaic modules by electrostatic separation. J Sustain Metall 4(2):176–186
3. Ministry of the Environment Government of Japan (2016). http://www.env.go.jp/press/files/jp/102441.pdf. (Accessed 20 Jun 2022)
4. Doi T, Tsuda I, Unagida H, Murata A, Sakuta K, Kurokawa K (2001) Experimental study on PV module recycling with organic solvent. Sol Energy Mater Sol Cells 67(1–4):397–403
5. New Energy and Industrial Technology Development Organization (NEDO) (2019) https://www.nedo.go.jp/content/100901845.pdf . (Accessed 20 Jun 2022)
6. Matsubara T, Uddin MA, Kato Y, Kawanishi T, Hayashi Y (2018) Chemical treatment of copper and aluminum derived from waste crystalline silicon solar cell modules by mixed acids of HNO_3 and HCl. J Sustain Metall 4:378–387
7. Takami K, Kobashi M, Shiraga Y, Uddin MA, Kato Y, Wu S (2015) Effect of HF and HNO_3 concentration on etching rate of each component in waste crystalline silicon solar cells. Mater Trans 56(12):2047–2052
8. Klugmann-Radziemska E, Ostrowski P (2010) Chemical treatment of crystalline silicon solar cells as a method of recovering pure silicon from photovoltaic modules. Renew Energ 35(8):1751–1759
9. Truc NTT, Lee B-K (2016) Sustainable and selective separation of PVC and ABS from a WEEE plastic mixture using microwave and/or mild-heat treatment with froth flotation. Environ Sci Technol 50:10580–10587
10. Mallampati SR, Lee C-H, Park MH, Lee B-K (2018) Processing plastics from ASR/ESR waste: separation of poly vinyl chloride (PVC) by froth flotation after microwave-assisted surface modification. J Mater Cycles Waste Manag 20:91–99
11. Qu YH, Li YP, Zou XT, Xu KW, Xue YT (2021) Microwave treatment combined with wetting agent for an efficient flotation separation of acrylonitrile butadiene styrene (ABS). J Mater Cycles Waste Manag 23:96–106
12. Wang C, Wang H, Fu J, Zhang L, Luo C, Liu Y (2015) Flotation separation of polyvinyl chloride and polyethylene terephthalate plastics combined with surface modification for recycling. Waste Manag 45:112–117
13. Wang J, Wang H, Wang C, Zhang L, Wang T, Zhang L (2017) A novel process for separation of hazardous poly (vinyl chloride) from mixed plastic wastes by froth flotation. Waste Manag 69:59–65
14. Li W, Li Y (2022) Selective flotation separation of polycarbonate from plastic mixtures based on Fenton treatment combined with ultrasonic. J Mater Cycles Waste Manag 24:917–926
15. Ito M, Takeuchi M, Saito A, Murase N, Phengsaart T, Tabelin CB, Hiroyosshi N, Tsunekawa M (2019) Improvement of hybrid jig separation efficiency using wetting agents for the recycling of mixed-plastic wastes. J Mater Cycles Waste Manag 21:1376–1383
16. Ito M, Saito A, Murase N, Phengsaart T, Kimura S, Kitajima N, Takeuchi M, Tabelin CB, Hiroyosshi N (2020) Estimation of hybrid jig separation efficiency using a modified concentration criterion based on apparent densities of plastic particles with attached bubbles. J Mater Cycles Waste Manag 20:2071–2080
17. Jiang H, Zhang Y, Bian K, Wang H, Wang C (2022) Insight into the effects of aqueous species on microplastics removal by froth flotation: kinetics and mechanism. J Environ Chem Eng 10:107834
18. Zhang Y, Jiang H, Bian K, Wang H, Wang C (2021) A critical review of control and removal strategies for microplastics from aquatic environments. J Environ Chem Eng 9:105463
19. Eivazihollagh A, Tejera J, Svanedal I, Edlund H, Blanco A (2017) Removal of Cd^{2+}, Zn^{2+}, and Sr^{2+} by ion flotation, using a surface-active derivative of DTPA (C12-DTPA). Ind Eng Chem Res 56:10605–10614

20. Cao D, Xu X, Jiang S (2021) Ultrasound-electrochemistry enhanced flotation and desulfurization for fine coal. Sep Purif Technol 258:117968
21. Jatav PP, Tajane SP, Mandavgane SA, Gaidhani SB (2019) A process of carbon enrichment of bottom slag ash for value-added applications. J Mater Cycles Waste Manag 21:539–546
22. Xie Q, Wang D, Han Z, Tao H, Liu S (2022) Removal of carbon and dioxins from municipal solid waste incineration fly ash by ball milling and flotation methods. J Mater Cycles Waste Manag. https://doi.org/10.1007/s10163-022-01514-6
23. Altansukh B, Burmaa G, Nyamdelger S, Ariunbolor N, Shibayama A, Haga K (2014) Gold recovery from its flotation concentrate using acidic thiourea leaching and organosilicon polymer. Int J Soc Mater Eng Resour 20:29–34
24. Burat F, Demirag A, Safak MC (2020) Recovery of noble metals from floor sweeping jewelry waste by flotation-cyanide leaching. J Mater Cycles Waste Manag 22:907–915
25. Dinc NI, Tosun AU, Basturkcu OM, Burat F (2022) Recovery of valuable metals from WPCB fines by centrifugal gravity separation and froth flotation. J Mater Cycles Waste Manag 24:224–236
26. Harada S, Uddin MA, Kato Y, Kawanishi T, Hayashi Y (2019) Separation between silicon and aluminum powders contained within pulverized scraped silicon-based waste solar cells by flotation method. J Sustain Metall 5:551–560
27. Park C-H, Subasinghe N, Han O-H (2015) Amenability testing of fine coal beneficiation using laboratory flotation column. Mater Trans 56:766–773
28. Vinett L, Waters KE (2020) Representation of kinetics models in batch flotation as distributed first-order reactions. Minerals 10:913
29. Matsuoka H, Mitsuhashi K, Kawata M, Tokoro C (2020) Deviation of flotation kinetic model for activated and depresses copper sulfide minerals. Minerals 10:1027
30. Javanovic I, Miljanovic I (2015) Modelling of flotation processes by classical mathematical methods- a review. Arch Min Sci 60:905–919
31. Gharai M, Venugopal R (2016) Modeling of flotation process – an overview of different approaches. Miner Process Extr Metall Rev 37:120–133
32. Wang L, Peng Y, Runge K, Bradshaw D (2015) A review of entrainment: mechanisms, contributing factors and modelling in flotation. Miner Eng 70:77–91
33. Imaizumi T, Inoue T (1961) A study of flotation as a rate process. J Min Metall Inst Jpn 77:987–994
34. Nguyen AV, Harvey PA, Jameson GJ (2003) Influence of gas flow rate and frothers on water recovery in a froth column. Miner Eng 16:1143–1147
35. Takamori T, Fukami S (1970) New method for evaluation of the flotation characteristics of ore. Flotation 41:1–7